

## A precast slab track partially reinforced with GFRP rebars

Seung-Jung Lee<sup>1a</sup>, Do-Young Moon<sup>\*2</sup>, Chi-Hyung Ahn<sup>1a</sup>, Jong-Woo Lee<sup>3b</sup> and Goangseup Zi<sup>4b</sup>

<sup>1</sup>Korea Railroad Research Institute, 176 Cheoldobangmulgwan-ro, Uiwang, Gyeonggi-do 16105, Republic of Korea

<sup>2</sup>Department of Civil Engineering, Kyungsung University, 309 Suyeong-ro, Nam-gu, Busan 48434, Republic of Korea

<sup>3</sup>Department of Railway Electrical & Signaling Engineering, Seoul National University of Science and Technology,  
232 Gongneung-ro, Nowon-gu, Seoul 01811, Republic of Korea

<sup>4</sup>School of Civil, Environmental & Architectural Engineering, Korea University, 145 Anam-ro, Seongbuk-gu, Seoul 02841, Republic of Korea

(Received March 16, 2017, Revised October 19, 2017, Accepted November 13, 2017)

**Abstract.** This study developed and investigated a precast slab track system partially reinforced with glass fiber reinforced polymer (GFRP) rebars in the transverse direction, which mitigated the loss of track circuit current by reducing magnetic coupling between the rails and steel reinforcements. An electric analysis was conducted and the results of the analysis verified that the GFRP rebars mitigate the reduced current strength produced by electro-magnetic induction. In the study, a three-dimensional finite element method and flexural experiments were used to study the mechanical behavior of the proposed slab track.

**Keywords:** slab track; concrete; track circuit current; magnetic coupling; glass fiber reinforced polymer (GFRP)

### 1. Introduction

Over the past two decades, concrete slab track systems have replaced traditional ballasted track systems. This was especially applicable in the case of high-speed railway systems, which demand a high level of track quality, long service life, and low maintenance cost (Tayabji and Bilow 2001, Zi *et al.* 2012, Pratico and Giunta 2016, Shi *et al.* 2016, Giannokos 2016, Ugarte *et al.* 2017). Concrete slab track systems may be classified into two different types according to the construction method used—cast-in-place systems and precast systems. The former system involves assembling precast concrete sleepers and reinforcement bars in the field and casting the concrete in the form of tracks that integrate the sleeper and the reinforcement bars. The reinforcement bars are usually placed in both the longitudinal direction as well as the transverse direction. Examples of cast-in-place systems include Rheda, Züblin, Stedef, Sonnevile, and SBB (Bachmann 2006, Michas 2012, Gautier 2015). Quality control is important in this system, and this in turn is significantly influenced by the field condition similar to asphalt pavement (Lee *et al.* 2015).

Conversely, precast systems produce relatively high quality slab tracks as compared with the cast-in-place systems. Additionally, maintenance costs can be reduced in precast systems (Lichtberger 2005). In the precast system, the track consists of many precast modules that are pre-fabricated in a factory prior to the construction. Therefore,

the quality control of the slab track exceeds that of the cast-in-place system. Examples of precast systems include Bögl, IPA, Ö BB-Porr, and Shinkansen slab track (J-slab) (Ando *et al.* 2001, Bachmann 2006, Michas 2012, Gautier 2015).

The railway signaling system controls train speed, train-to-train distance, and routes, and therefore plays an important role in maintaining the efficiency of the railway system. The railway signaling system transmits train control information pertaining to the location and speed limit of trains by using automatic train control (ATC), automatic train protection (ATP), or automatic train stop (ATS) systems. Signaling systems may be classified into the following three types based on the manner in which train control information is transmitted: (1) on-board systems that directly use the track (ATC system), (2) establishment of an instrument on the track, and (3) establishment of an instrument on the trackside such as traffic lights (ATS and ATP systems). Particularly, the ATC system that directly uses the track as a conductor for a part of the track circuit to transmit control signals is used in Korean high-speed railway systems (Posluszny 2016).

The track circuits are operated by sensors that detect the electric current passing through the rails on the slab track. However, concrete slab tracks have several steel reinforcements to stably resist loads as shown in Fig. 1. These tracks could negatively influence the track circuits employed by train control systems (Theeg and Vlasenko 2009). The currents flowing on the rails produce electro-magnetic fields in which several magnetic couplings occur between the rails and steel reinforcements. These magnetic couplings generate several small circulation currents in the steel reinforcements, which in turn consume the electric power of the track circuit. This issue exists in both cast-in-place and precast slab track systems.

Generally, insulating joints made of wood or plastic

\*Corresponding author, Associate Professor

E-mail: [dymoon@ks.ac.kr](mailto:dymoon@ks.ac.kr)

<sup>a</sup>Senior Researcher

<sup>b</sup>Professor



Fig. 1 Steel reinforcements in the concrete slab track system

material are installed between two adjacent steel reinforcements to overcome the aforementioned loss of track circuit current due to magnetic coupling (Lichtberger 2005) as shown in Fig. 1. In Korea, both cast-in-place and precast slab track systems require a considerable amount of insulation work involving plastic blocks or rubber hoses at the contact points of the steel reinforcements (approximately 700 points per slab track). Despite the advantage of insulation, it was observed that the use of the insulation caused a construction process delay and increased labor costs.

The primary objective of this study is to develop a precast slab track system for mitigating the losses of track circuit current by reducing magnetic coupling for high-speed railway systems. The paper is divided into the following sections: The design objective of the slab track and the structural design of the slab track are introduced in Section 2, the electrical and structural behavior of the proposed slab track is detailed in Section 3, and the structural experimental verifications are discussed in Section 4. The conclusions of this study are presented in Section 5.

## 2. Slab track system for mitigating track circuit current losses

### 2.1 Design objective of the slab track system for low track circuit current losses

A train control system using track circuits to detect train locations and transmit train control codes is important in the

development of the slab track system. In order to detect train control signals, the current flowing through the rails should be greater than the minimum level. In Korean high-speed railway systems, a modulated current is transmitted using a UM17C track circuit system. This modulated current should be maintained at a minimum level of 0.8 A to transmit the control signal to the trains at the end of the block. The standard block length is approximately 1,500 m (Kim *et al.* 2009).

Electro-magnetic theory suggests that a large amount of circulation current generated by the induced magnetic fields of the main current on the rail are produced on the reinforcements in different directions. The circulation currents disturb the main current flowing on the rail and shorten its transmission length. It was observed that the circulation currents could cause problems in the transmission of signal information of the trains. The number of the circulations and the circulation area should be reduced to mitigate the main current loss on the rail as the induced circulation current is proportional to the cross sectional area of its circulation (Hill 1993).

Fig. 2 shows the three steps involved in minimizing the circulation current effects: (1) a general rectangular-shaped slab track is selected as shown in Fig. 2(a), (2) a frame-shaped slab track in which the internal induced circulation loops inside the rails are removed to mitigate the induced currents inside the rails, is selected as shown in Fig. 2(b), and (3) the proposed electrical insulators are used instead of the steel reinforcements in a transverse direction, and finally, all the circulation loops inside the rails as well as the big loop are removed as shown in Fig. 2(c). In this study, a frame-shaped slab track reinforced with electrical insulators in the transverse direction was developed to mitigate the induced current effect caused by the steel reinforcements. It was expected that the developed frame-shaped slab track could reduce the insulation works during the construction process and could reduce the construction expense.

### 2.2 Frame-shaped slab track reinforced with GFRP rebars

Glass fiber reinforced polymers (GFRP) are widely used for construction applications in civil engineering (Bakis *et al.* 2002). Although the weight of GFRP does not exceed one fourth the weight of the steel reinforcements, the

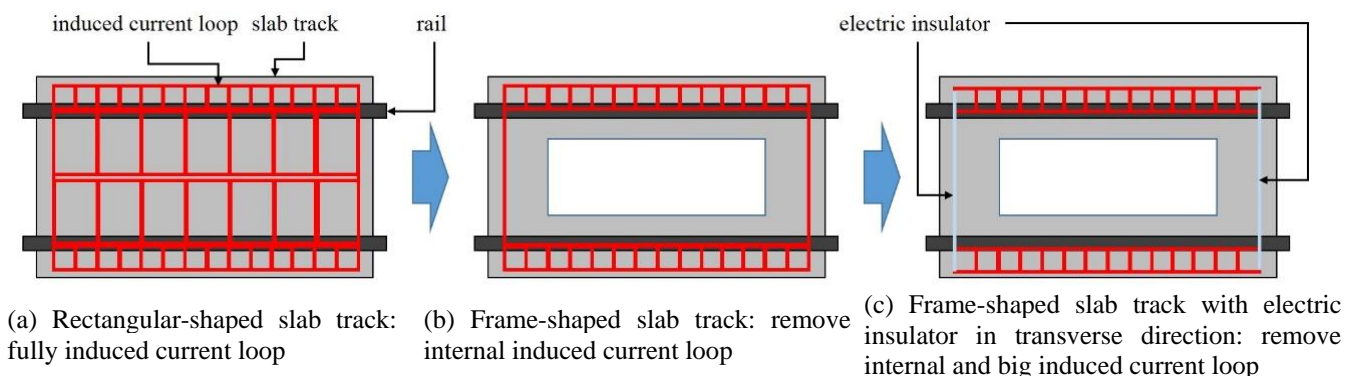


Fig. 2 Design objective of slab track system to reduce induced current loop by steel reinforcements

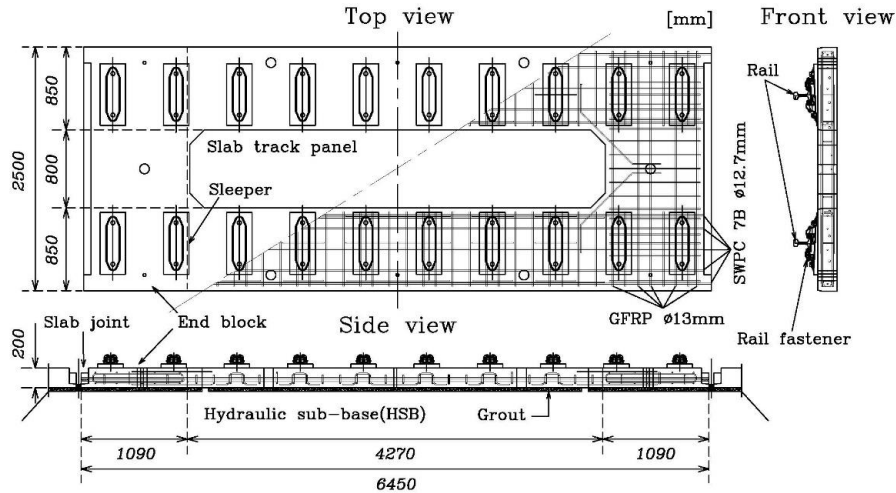


Fig. 3 The precast concrete slab track considered in this paper

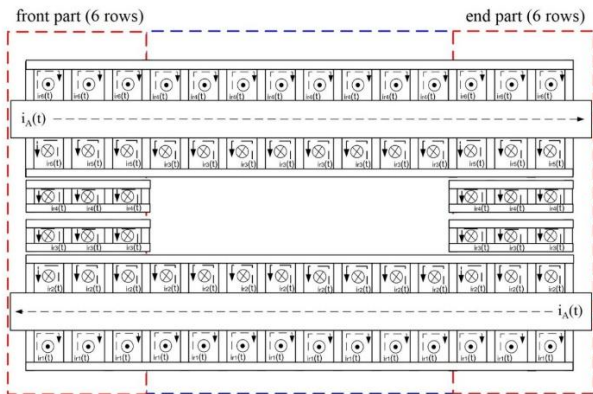


Fig. 4 Induced current loop for the slab track considered in this paper

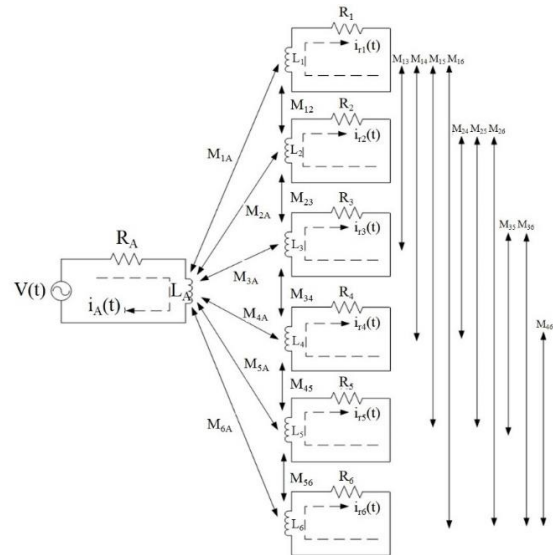


Fig. 5 Electrically equivalent model of the front and end parts of the slab track

strength of GFRP is twice that of the steel reinforcements. Furthermore, GFRP is an excellent electric insulator. With respect to the internal reinforcements in concrete structures, commercially available GFRP rebars could be a promising alternative to steel reinforcements because of its improved corrosion resistance and strength (Bakis *et al.* 2002, Hao and Zhang 2016). Many surface types of GFRP rebars such as braided or wrapped GFRP rebars with fibers or roughened GFRP rebars were developed to enhance the bond with concrete (DongWon 2004).

This study proposed a slab track reinforced with GFRP rebars with improved electric insulating properties. The precast slab track reinforced with GFRP rebars consisted of a rail, rail fasteners, sleepers, a reinforced concrete slab track panel, a hydraulic sub-base (HSB), a slab joint, and a grout layer as shown in Fig. 3. The figure also provides geometric details. The concrete slab track panel was typically separated from the HSB with a grout layer made of cement asphalt mortar (Bilow and Randich 2000, Tayabji and Bilow 2001, Giannokos 2016). The developed slab track panel was reinforced with GFRP rebars for the purpose of insulation as well as to resist loads. A large number of steel reinforcements and pre-stressing tendons were essentially installed inside panels to resist numerous loads applied to the system.

### 3. Behavior of the slab track with GFRP rebars

#### 3.1 Electrical behaviour of the slab track

##### 3.1.1 Development of the numerical model

The electro-magnetic fields from the rail current generates the induced currents on the reinforcements. In this study, based on the finite element method, a commercial electro-magnetic simulator MAXWELL was used for investigating the effect of the induced currents. The mutual impedance of the rail was also analytically calculated by using a transformer model. The slab track could be simply considered as several small loops as shown in Fig. 4. In the front and end parts of the loop model of a GFRP slab track, steel reinforcements produced six rows of the induced current loops. The six rows of the current loops could be represented as electrically equivalent models as shown in Fig. 5.

In Fig. 5,  $v(t)$ ,  $R_A$ , and  $i_A(t)$  denote voltage, resistance, and current in the track circuit, respectively.

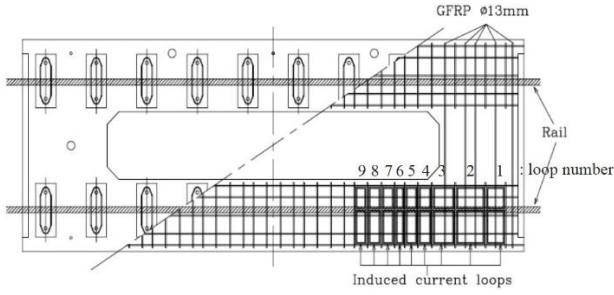


Fig. 6 Nine different current loops in the slab track considered in this paper

Additionally,  $i_{rp}$  and  $R_p$  denote current and resistance in the reinforcement  $p$ , respectively. Furthermore,  $L_A$  and  $L_p$  denote self-inductances of the rail and the reinforcement  $p$ , respectively, and  $M_{pA}$  and  $M_{pq}$  denote mutual inductance between the rail and the reinforcement  $p$ , and mutual inductance between the reinforcements  $p$  and  $q$ , respectively. As shown in Fig. 5, the impedance of the rail can be calculated by using Kirchhoff's law and Euler's law as shown in Eq. (1).

$$Z = \frac{V}{I_A} = k_1 - k_2 - k_3 - k_4 - k_5 - k_6 - k_7 \quad (1)$$

$$k_1 = R_A + j\omega L_A \quad (2)$$

$$k_{p+1} = j\omega M_{pA} H_p \text{ for } p = 1, 2, \dots, 6 \quad (3)$$

where  $\omega$  and  $H_p$  denote current frequency, and current ratio matrix, respectively. The values of the coefficients

used in this study are from the report on the Korean high-speed railway system by Sampyo E&C (2011). The rail resistance represented in Eq. (4) constitutes the real part of Eq. (1) and the inductance represented in Eq. (5) represents the imaginary part of Eq. (1) divided by frequency  $\omega$  as follows.

$$R = \text{real}(Z) \quad (4)$$

$$L = \frac{\text{imag}(Z)}{\omega} \quad (5)$$

### 3.1.2 Results of the electrical analysis

The rail impedances depend on the area of the induced loop caused by the steel reinforcements because they are induced in different current loop surfaces. There are nine cases in the developed slab track panel as shown in Fig. 6

The resistance and inductance of the slab track were calculated by using MAXWELL with the electric models as shown in Fig. 7. Finally, the main current strength along the track was obtained at the carrier frequencies of the Korean high-speed railway track circuit with 2040, 2400, 2760, and 3120 Hz as shown in Fig. 8.

The minimum current value required to transmit the control information along the track is 0.8A. In the case of the higher frequency for the slab track without GFRP rebars, the current was unable to reach 1500 m with the required values due to several induced small loop currents between the rail and steel reinforcements as shown in Fig. 8(a). It was observed that the current strength was below 0.8A near 1200 m for the carrier frequency of 3120 Hz. On the other hand, in the case of all frequencies for the slab

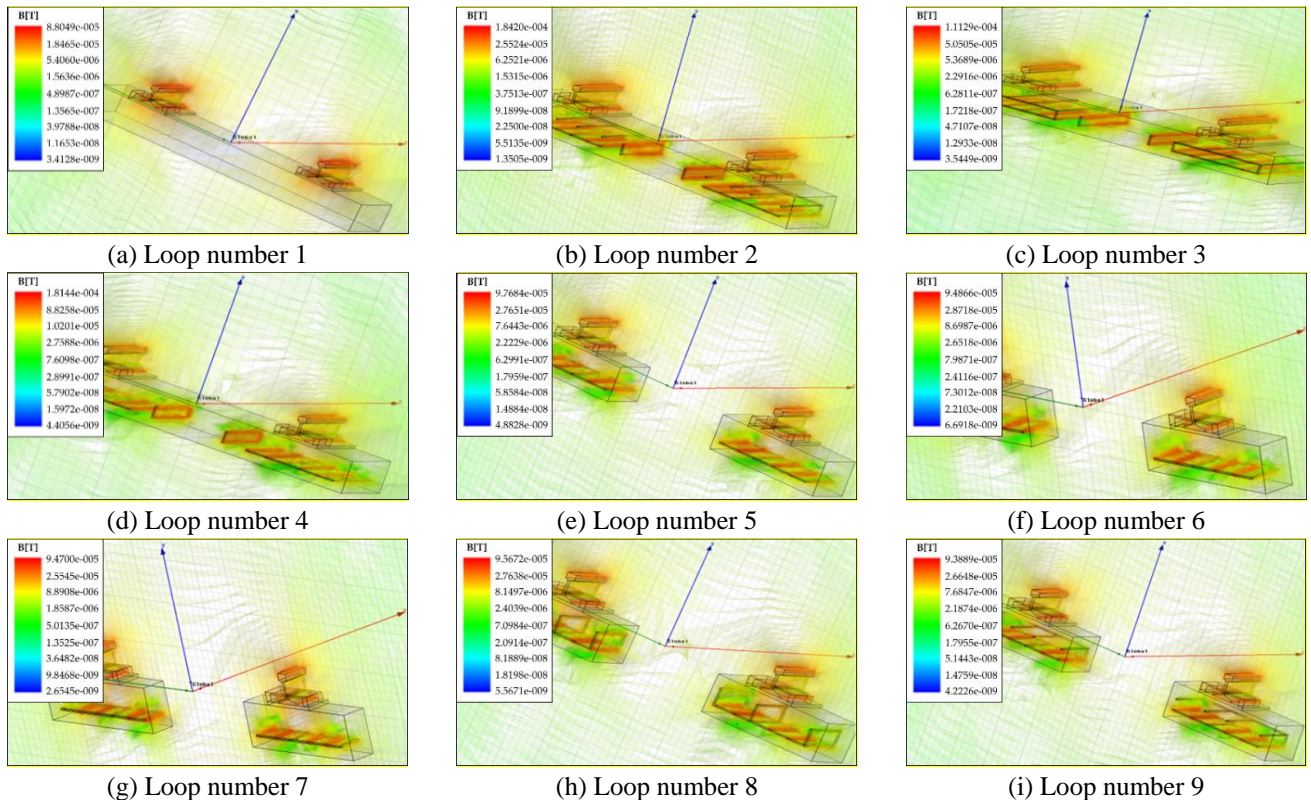


Fig. 7 Three dimensional electromagnetic modeling results

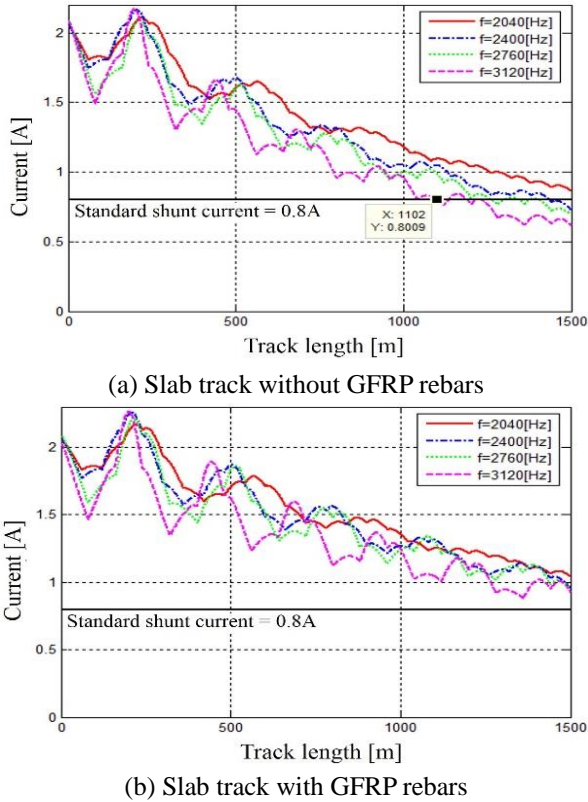


Fig. 8 Simulation results of current strength along a track circuit rail

track with GFRP rebars, the current strength at all four different frequencies exceeded 0.8 A along the track as shown in Fig. 8(b). The minimum shunt current was 0.85A at 1420 m for the carrier frequency of 3120 Hz. It could be observed that the level of shunt current in the case of all frequencies for the slab track with GFRP rebars satisfied the requirement of exceeding 0.8A along the track length of 1500 m due to the mitigation of the induced currents.

In addition, it would be helpful if the experimental verification for electrical behavior of proposed slab track system is investigated. Further study about the experiments requiring only inexpensive cost will be carried out.

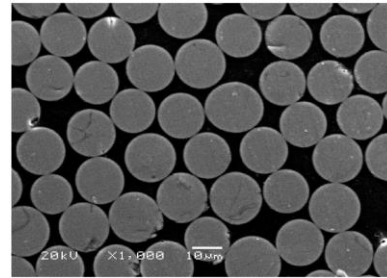
### 3.2 Mechanical behavior of the slab track

#### 3.2.1 Material properties of GFRP rebars

GFRP bars of 13 mm diameter were used as reinforcement for the slab track. These rebars were commercially manufactured in Korea and had long glass fibers wrapping the surface of the rebars as shown in Fig. 9 (DongWon 2004, Oh *et al.* 2009). All the mechanical properties of the GFRP rebar were measured based on standard tests in ACI 440.3R-12 (ACI 2012). The data of the tensile tests of a GFRP rebar is shown in Table 1. The guaranteed tensile strength  $f_{fu}^*$  of the FRP bar can be defined in terms of the mean tensile strength  $f_{u,ave}$  minus three times the standard deviation (ACI 2015). In this study, the guaranteed tensile strength of a GFRP rebar with 13 mm diameter was 1052 MPa. The design tensile strength considering reductions for service environments can be



(a) Shape of GFRP rebar



(b) SEM image of GFRP

Fig. 9 Simulation results of current strength along a track circuit rail

Table 1 Data of tensile test of GFRP rebar

	Tensile strength [MPa]	Ultimate strain [%]	Tensile modulus of elasticity [GPa]
GFRP-1	1084.8	2.027	53.4
GFRP-2	1109.6	2.192	51.2
GFRP-3	1118.3	2.217	50.1
Average	1104.3	2.150	51.6
Standard deviation	17.4		1.7

determined by the following equation.

$$f_{fu} = C_E f_{fu}^* \quad (6)$$

in which  $f_{fu}$  represents the design tensile strength and  $C_E$  represents the environmental reduction factor for various fiber types and exposure conditions. When the concrete was exposed to earth and weather, the  $C_E$  value was 0.7. Therefore, the design tensile strength used in this study was 736.4 MPa. The fatigue strength was 20% of the design tensile strength, which was equal to 147.3 MPa and the specified tensile modulus was 51.6 GPa.

#### 3.2.2 Development of the three-dimensional finite element model

A few design methodologies for precast slab track systems were proposed by previous studies. However, most of these methodologies use Westergaard's solution for concrete pavements based on the plate on the Winkler type elastic foundation to calculate stress (Westergaard 1926, 1933, 1948, Giannokos 2016). The use of this solution is limited to plate type slab track system, which is not suitable for different shapes such as a frame-shaped slab track. In this study, a three-dimensional finite element model was developed instead of using Westergaard's solution as in the case of the J-slab in Japan (Zi *et al.* 2012, Awad and Yusaf

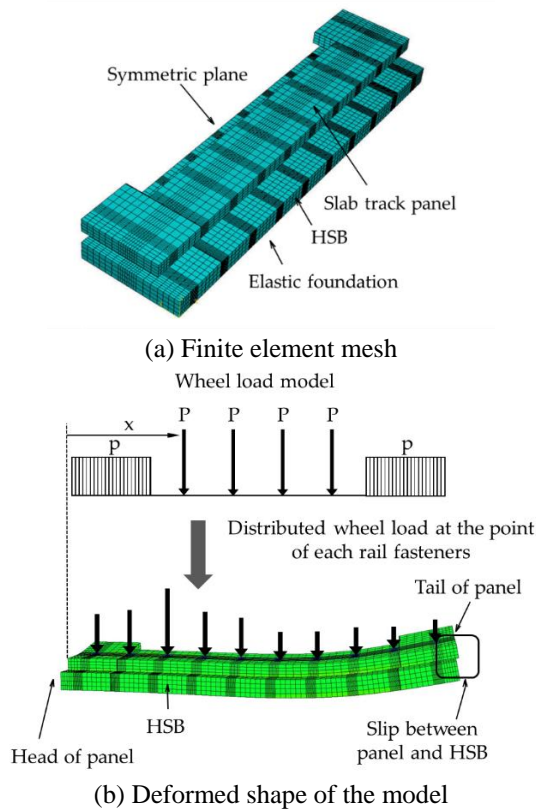


Fig. 10 The three dimensional finite element model

2012, Michas 2012, Gautier 2015, Poveda *et al.* 2015, Giner *et al.* 2016).

Fig. 10(a) shows the three-dimensional finite element mesh used in the analysis. The models were implemented by using a commercial software ABAQUS (ABAQUS 2005). The slab track considered in this study was rather long in proportion to its thickness. Therefore, a C3D8I (with an 8-node linear brick and incompatible modes) element, which improves the bending behavior was used for this structure (ABAQUS 2005). Only half of the panel and HSB were meshed as shown in Fig. 10(a) due to the symmetry in the transverse direction of the slab track panel and HSB. The slab track panel has 34.5 GPa of elastic modulus and 40 MPa of compressive strength. The HSB has 12.9 GPa of elastic modulus for conservative design of slab track.

This structure had a grout layer between the slab track panel and HSB as shown in Fig. 3. This grout layer used small holes in the panel to fill a vacuum after the installation of the slab track panel. This structure could be considered as consisting of two different systems based on the effect of the grout layer, namely (1) without bonding and (2) with bonding between the slab track panel and HSB layer (Eisenmann 2000, 2006). In this study, the bonding effect by the grout layer could be neglected based on the conservative aspect of the design viewpoint, and thus the grout layer was removed during the analysis. Therefore, the slab track panel and HSB were modeled separately. Any interpenetrating displacements between the slab track panel and HSB were not allowed, and slip as well as relative displacements between these two layers were considered.

Table 2 Stresses calculated considering the movement of axle loads

	Stress in longitudinal direction [MPa]	Stress in transverse direction [MPa]
Load case 1 ( $x=0$ )	1.424	1.478
Load case 2 ( $x=150$ )	1.395	1.532
Load case 3 ( $x=300$ )	1.267	1.541
Load case 4 ( $x=450$ )	1.090	1.476
Load case 5 ( $x=600$ )	0.956	1.405
Maximum	1.424	1.541

The rail and rail fasteners were not considered in the three dimensional analysis. Thus, the wheel load is considered to be distributed at the position of each rail fasteners as follows: (1) The wheel load based on UIC 71 load model is distributed to the rail. (2) The deflection of rails is calculated based on the well-known beam on elastic foundation theory of Winkler, Eq. (7). (3) The supporting reactions on each rail fasteners are calculated by rail deflection and the stiffness of rail fasteners. (4) Then, the calculated reactions are applied at the position of each rail fasteners as shown in Fig. 10(b).

The behavior included both non-interpenetrating and relative displacements between two layers as shown in Fig. 10(b). The HSB layer was assumed as supported by an equivalent Winkler spring. The stiffness of the spring was calculated based on the Winkler foundation type.

### 3.2.3 Results of the analysis

The calculated stresses considering the movement of the wheel load of the train are shown in Table 2. The UIC 71 load model with four 250 kN axle loads and a distributed load of 80 kN/m was used for the wheel load of a train, and this axle load was distributed by the rail to rail fasteners on the slab track panel (UIC 2001). The movement of the wheel load was considered as the distance between the head of the panel and the first of the four axle loads which is " $x$ " in Table 2 as shown in Fig. 10(b). All load cases are listed in Table 2. In the design, the maximum stresses in both directions were multiplied by the factor, 1.529, that accounted for the effect of dynamic impact based on the numerous field surveys (KR C-14060 2014).

Figs. 11(a) and (b) show the contour plots of the stresses in the longitudinal and transverse directions, respectively. The maximum longitudinal stress occurred at a point two thirds of the distance along the longitudinal direction where the slab track panel was bent. Additionally, the maximum transverse stress occurred below the first rail fastener from the head of the panel. The maximum stress in the transverse direction exceeded that in the longitudinal direction as listed in Table 2. The amount of reinforcements was determined based on these results.

The design of the reinforcements in this slab track was based on ACI 318-14 and 440.1R-15 (ACI 2014, 2015). In the transverse direction, if the GFRP rebars resisted the maximum tensile stress that occurred beneath the first rail fastener from the head of the panel, then the minimum requirements of the GFRP rebars increased significantly and the development length could not be satisfied. Therefore,

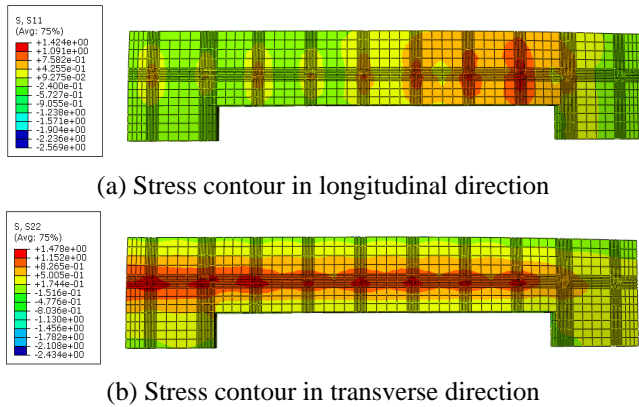


Fig. 11 The results of three dimensional finite element analysis

the steel reinforcements resisted the maximum tensile stress that occurred in the end block, and the GFRP rebars only resisted the stress of 0.4MPa that occurred in the middle of the end block in the transverse direction.

The reinforced amount of the GFRP rebars was determined based on the serviceability condition, control of cracks, and creep rupture. The maximum allowable crack width was 0.5 mm for exterior exposure (ACI 2014). Additionally, if the structure reinforced with the GFRP rebars was subjected to fatigue loading, then the stress of the GFRP rebars should be limited to the 20% of the design tensile strength or  $f_{fu}$ , which is equal to 148.3 MPa (ACI 2015). Therefore, five GFRP rebars with 13 mm diameter were distributed in the end block. Top and bottom concrete covers of 40mm diameter were used.

#### 4. Experimental verification of the mechanical behavior of the slab track

##### 4.1 Mechanical behavior of the slab track in the longitudinal direction

Four-point flexural tests were carried out to verify the mechanical behavior of the proposed slab track which is similar to the work of Tarifa et al. as shown in Fig. 12 (Tarifa et al. 2015). The two different types of test specimens based on the direction of the specimen cut from the slab track panel were as follows: (1) LF corresponds to the specimen cut in the longitudinal direction and (2) TF corresponded to the specimen cut in the transverse direction as shown in Figs. 12(a) and (c), respectively. In order to control for the possible random scattering of the test data, four test specimens of each type were prepared.

High-strength concrete with an average 28-day concrete compressive strength of 49.2 MPa based on the average values obtained from tests performed on 10×20 cm cylinders was used for the slab track panel. Linear Variable Differential Transformers (LVDTs) were designed to measure the mid-point displacement as shown in Figs. 12(a) and (c). The transformers were installed on the angle steel placed on the roller supports to remove all unnecessary displacements except that of the test specimens. The load

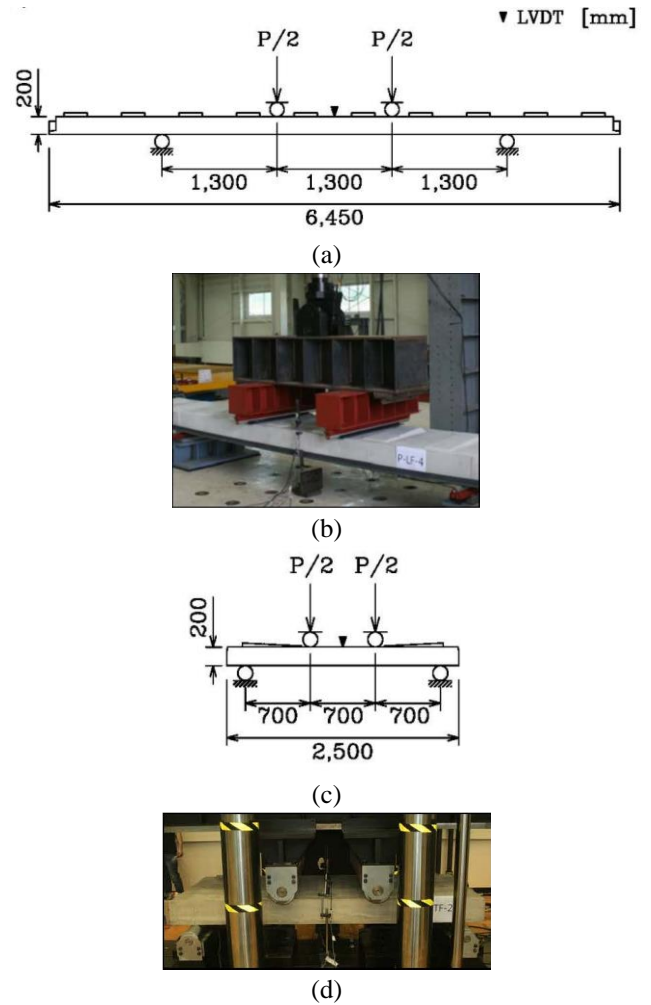
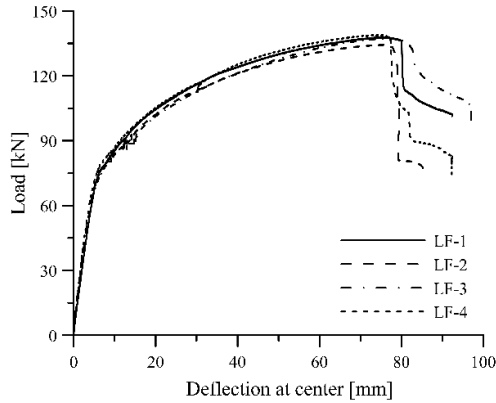


Fig. 12 The specimens details & experiment setup of the flexural tests: (a) test specimen of LF which is in longitudinal direction, (b) test setup of LF, (c) test specimen of TF which is in transverse direction, and (d) test setup of TF

was applied to the specimens through two equal rollers attached to the actuator at distances of 1,300 mm and 700 mm from each support to avoid the sleepers.

An MTS actuator and a Samyeon servohydraulic actuator were used for the testing. The actuators were capable of applying 250 kN of axial force. All tests were performed by a displacement control method at a rate of 2 mm/min until the applied load decreased. The cracks and displacements were checked and plotted as each crack occurred. All data was captured on a computer that used a Tokyo Sokki TDS-303 data acquisition system.

The load-displacement curves for the specimens in the longitudinal direction are shown in Fig. 13(a). The load increased linearly to a maximum of approximately 75 kN when the displacement at the mid-point was approximately 10mm. Following this, the hardening started as the load increased nonlinearly up to a maximum load of approximately 135 kN when the displacement at the mid-point was approximately 75 mm. After reaching the maximum load, the load decreased significantly with the failure of the specimen. The average flexural strength was



(a) load-displacement curves



(b) failure patterns

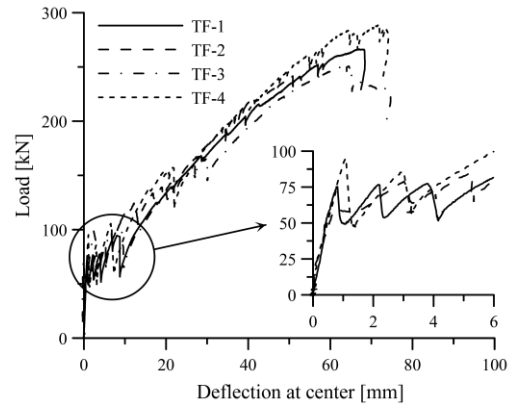
Fig. 13 The test data of the flexural tests in longitudinal direction

Table 3 Data of the flexural specimens

Direction	Specimens	Maximum load [kN]	Failure displacement [mm]	Flexural strength [kN m]
Longitudinal	LF-1	137.87	74	89.62
	LF-2	134.31	76	87.30
	LF-3	137.38	75	89.30
	LF-4	138.82	73	90.23
	Average	137.10	75	89.11
	Average/Nominal	-	-	1.5 (89.11/59.53)
Transverse	TF-1	266.08	68	93.13
	TF-2	250.83	64	87.79
	TF-3	284.18	74	99.46
	Average	267.03	69	93.46
	Average/Nominal	-	-	1.15 (93.46/81.35)

89.11 kNm, which was approximately 1.5 times that of the nominal strength of 59.53 kNm. The first crack began to appear between the loading points at a displacement of 10mm. Finally, several flexural cracks grew and resulted in the concrete crushing at the top of the specimen that was under the loading points as shown in Fig. 13(b). The results confirmed that the developed slab track had sufficient flexural strength in the longitudinal direction because it was approximately 1.5 times that of the nominal strength. All the data are shown in Table 3.

#### 4.2 Mechanical behavior of the slab track in the transverse direction



(a) load-displacement curves



(b) failure patterns

Fig. 14 The test data of the flexural tests in transverse direction

The load-displacement curves for the specimen in the transverse direction are shown in Fig. 14(a). The load increased linearly to approximately 70 kN when the displacement at the mid-point was approximately 5 mm, and then the load decreased and increased repeatedly for a few times. This situation could be caused by the squeezing through of the GFRP rebars, and not due to the failure of the GFRP surface. The GFRP rebar at the position in which the cracks occurred squeezed through the concrete due to its low stiffness in the radial direction (Fib 2000). A finite element analysis indicated that the vertical deflection of the slab track panel was almost 1mm when the service load was applied to the developed slab track on the elastic foundation. Giannokos also published 0.37 mm deflection of concrete slab under the service load condition (Giannokos 2016). Given these results, squeeze through was not expected to occur in slab track panels reinforced with GFRP rebars during the service life. Furthermore, in the event of squeeze through during the service life, there is no structural problem because the GFRP rebars have sufficient development length to retain the flexural strength. Following this, the load increased nonlinearly up to a maximum load of approximately 265 kN when the displacement at the mid-point was approximately 70 mm. The load decreased after the maximum load was reached. Average flexural strength was 93.46 kNm, which was approximately 1.15 times the nominal strength of 81.35 kNm. In the linear region, the panel in the transverse direction behaved linearly up to 75.3 kN (26.36 kNm). This corresponded to the cracked strength, which was the same as the modulus of rupture. This was approximately thrice

that of the factored flexural moment of 8.195 kNm. The crack patterns are shown in Fig. 14(b). The first crack began to appear between the loading points at a displacement of 5 mm. Several cracks grew to the top of the specimen and concrete crushed at a displacement of 70 mm. As expected, the flexural strength in the transverse direction exceeded the nominal strength as shown in Table 3.

## 5. Conclusions

The conclusions of the study are as follows:

- A precast slab track reinforced with GFRP rebars was developed to minimize the losses of track circuit current by reducing the magnetic coupling between the rails and steel reinforcements. In the study, a frame-shaped slab track reinforced with an electrical insulator with GFRP rebars in the transverse direction was developed to minimize the area of the induced current loop to mitigate the induced current effect.
- An electric simulation was used to verify the effect of the GFRP rebars in the developed slab track. All currents at different working frequencies in the case of the slab track with the GFRP rebars exceeded 0.8A at the block length of 1,500m. The findings indicated that the proposed slab track decreased the magnetic coupling when compared with that of the slab track panel with only steel reinforcements
- A finite element model was used to study the mechanical behavior of the slab track by considering the movement of the axle loads. The maximum stress in the transverse direction exceeded that in the longitudinal direction. In the proposed slab track, the GFRP rebars resisted the transverse stress at the end block of the slab track. The reinforced amount of the GFRP rebars was determined based on the serviceability condition, control of the cracks, and fatigue strength.
- In the longitudinal direction, the average flexural strength of the slab track was approximately 1.5 times that of the nominal strength, and in the transverse direction, the average flexural strength was approximately 1.15 times that of the nominal strength, and the crack strength was approximately 3 times the factored flexural moment.

## Acknowledgments

This research was supported by a grant (17CTAP-C117247-02) from Technology Advancement Research Program funded by Ministry of Land, Infrastructure and Transport of Korean government. The fifth author (G. Zi) appreciates the financial support by Basic Science Research Program through the National Research Foundation of Korea (NRF) funded by the Ministry of Science and ICT (NRF-2017R1A2B4002988). The assistance of Yeon-min Kwak and Sang-Soo Hwang for the experiment and Dong Won Construction Co. Ltd. for providing of GFRP rebars are appreciated.

## References

- ABAQUS (2005), Version 6.5 User's Manual, Hibbit, Karlson & Sorensen Inc.
- ACI 318-14 (2014), Building Code Requirements for Structural Concrete and Commentary, American Concrete Institute, USA.
- ACI 440.1R-15 (2015), Guide for the Design and Construction of Structural Concrete Reinforced with Fiber-Reinforced Polymer Bars, American Concrete Institute, USA.
- ACI 440.3R-12 (2012), Guide Test Methods for Fiber-Reinforced Polymers (FRPs) for Reinforcing or Strengthening Concrete Structures, American Concrete Institute, USA.
- Ando, K., Sunaga, M., Aoki, H. and Haga, O. (2001), "Development of slab track for Hokuriku Shinkansen lines", *Quart. Report. RTRI*, **42**(1), 35-41.
- Awad, Z.K. and Yusaf, T. (2012), "Fibre composite railway sleeper design by using FE approach and optimization techniques", *Struct. Eng. Mech.*, **41**(2), 231-242.
- Bachmann, H. (2006), *State-Of-The-Art: Ballastless Track Systems*, RTR Special, Slab Track.
- Bakis, C.E., Bank, L.C., Brown, V.L., Cosenza, E., Davalos, J.F., Lesko, J.J., Machida, A., Rizkalla, S.H. and Triantafillou, T.C. (2002), "Fiber-reinforced polymer composites for construction: State-of-the-Art review", *J. Compos. Constr.*, **6**(2), 73-87.
- Bilow, D.N. and Randich, G.M. (2000), "Slab track for the next 100 years", *Rail Transit Conference Proceedings*, 174-185.
- DongWon Construction Co. Ltd. (2004), <http://dwcons.com>, Guri, Gyenggi-do, Korea.
- Eisenmann, J. and Leykauf, G. (2000), *Beton Kalender*, Ernst & Sohn, Berlin, Germany.
- Eisenmann, J. and Leykauf, G. (2006), *Beton-Fahrbahnen*, 2nd Edition, Ernst & Sohn, Berlin, Germany.
- Fédération Internationale du Béton (fib) (2000), "Bond of reinforcement in concrete: state-of-art report", International Federation for Structural Concrete.
- Gautier, P.E. (2015), "Slab track: Review of existing systems and optimization potentials including very high speed", *Constr. Build. Mater.*, **92**, 9-15.
- Giannakos, K. (2016), "Deflection of a railway reinforced concrete slab track: Comparing the theoretical results with experimental measurements", *Eng. Struct.*, **122**, 296-309.
- Giner, I.G., Alvarez A.R., Garcia-Moreno, S.S.C. and Camacho, J.L. (2016), "Dynamic modelling of high speed ballasted railway tracks: Analysis of the behaviour", *Tran. Res. Procedia*, **18**, 357-365.
- Hao, H. and Zhang, C. (2016), *Mechanics of Structures and Materials: Advancements and Challenges*, FL, Taylor & Francis Group.
- Hill, R.J. (1993), "Rail track distributed transmission line impedance and admittance: Theoretical modeling and experimental results", *IEEE Tran. Veh. Rechnol.*, **42**(2), 225-241.
- Kim, M., Bae, Y., Lee, S. and Lee, J. (2009), "A study on electrical separation joint in the slab track", *International Conference in Electrical Machines and Systems*, Tokyo.
- KR C-14060 (2014), *Design of Track Materials*, Korea Rail Network Authority, Korea. (in Korean)
- Lee, S.J., Zi, G., Mun, S., Kong, J.S. and Choi, J.H. (2015), "Probabilistic prognosis of fatigue crack growth for asphalt concretes", *Eng. Fract. Mech.*, **141**, 212-229.
- Lichtberger, B. (2005), *Track Compendium*, Eurail Press.
- Michas G. (2012), "Slab track systems for high-speed railways", Master Thesis, Royal Institute of Technology, Stockholm, Sweden.
- Oh, H., Moon, D.Y. and Zi, G. (2009), "Flexural characteristics of concrete beams reinforced with a new type of GFRP bar", *Polym. Polym. Compos.*, **17**(4), 253-264.

- Posluszny, R.D. (2016), "Applications of prestressed AFRP bars in concrete railroad ties", Master Thesis, Texas A&M University, TX, USA.
- Poveda, E, Yu, R.C., Lancha, J.C. and Ruiz, G. (2015), "A numerical study on the fatigue life design of concrete slabs for railway tracks", *Eng. Struct.*, **100**, 455-467.
- Pratico, F.G. and Giunta, M. (2016), "Assessing the sustainability of design and maintenance strategies for rail track by means of life cycle cost analysis", *Proceedings of the 15<sup>th</sup> International Conference on Railway Engineering Design and Operation*, Madrid, Spain.
- Sampyo E&C (2011), "Evaluation of insulation performance of the precast slab track reinforced with GFRP rebars", Technical Report, Sampyo E&C. (in Korean)
- Shi, H, Yu, Z. and Shi, H. (2016), "An improved method for dynamic modelling of a slab track on a high-speed railway", *Proceedings of the 15<sup>th</sup> International Conference on Railway Engineering Design and Operation*, Madrid, Spain.
- Tarifa, M., Zhang, X., Ruiz, G. and Poveda, E. (2015), "Full-scale fatigue tests of precast reinforced concrete slabs for railway tracks", *Eng. Struct.*, **100**, 610-621.
- Tayabji, S.D. and Bilow, D. (2001), "Concrete slab track state of the practice", *Tran. Res. Record*, **1742**(1), 129-140.
- Theeg, G. and Vlasenko, S. (2009), *Railway Signalling & Interlocking*, Eurail Press, Hamburg.
- Ugarte, J., Carnerero, A. and Millanes, F. (2017), "Dynamic behavior of pergola bridge decks of high-speed railways", *Struct. Eng. Mech.*, **61**(1), 91-103.
- UIC 774-3R (2001), Track/brige Interaction Recommendations for Calculations, International Union of Railways, France.
- Westergaard, H.M. (1926), "Stresses in concrete pavements computed by theoretical analysis", *Pub. Road.*, **7**(2), 25-35.
- Westergaard, H.M. (1933), "Analytical tools for judging results of structural tests of concrete pavements", *Pub. Road.*, **14**(10), 185-188.
- Westergaard, H.M. (1948), "New formulas for stresses in concrete pavements of airfields", *Am. Soc. Civil Eng. Tran.*, **113**(2340), 425-444.
- Zi, G., Moon, D.Y., Lee, S.J., Jang, S.Y., Yang, S.C. and Kim, S.S. (2012), "Investigation of a concrete railway sleeper failed by ice expansion", *Eng. Fail. Anal.*, **26**, 151-163.